Robust PET-Based Chiral Schiff Base Molecular Probe for Recognition of Hg^{2+} and Pb^{2+} and Its Live Cell Imaging

S. Benita Jeba Silviya,[a] S. Michlin Ruphina Maragatham,[b] S.G. Jebastin Andrews,[c] Nattamai S.P. Bhuvanesh,[d] J. Winfred Jebaraj,[e] Chithiraivel Balakrishnan,[*,c]

[a]Department of Physics, Pope's College, Sawyerpuram - 628 251, Thoothukudi District, Tamil Nadu, India

[b]Department of Chemistry, Sarah Tucker College, Tirunelveli - 627 007, Tamil Nadu, India

[c]Department of Chemistry, Nazareth Margoschis College at Pillaiyanmanai, Nazareth - 628 617, Thoothukudi District, Tamil Nadu, India

[d]Department of Chemistry, Texas A&M University, College Station, TX 77843, USA

[e]Department of Chemistry, St. John's College, Tirunelveli - 627 002, Tamilnadu, India

*Corresponding Author

Tel: +91 7845061380

E-mail: balac0735@gmail.com

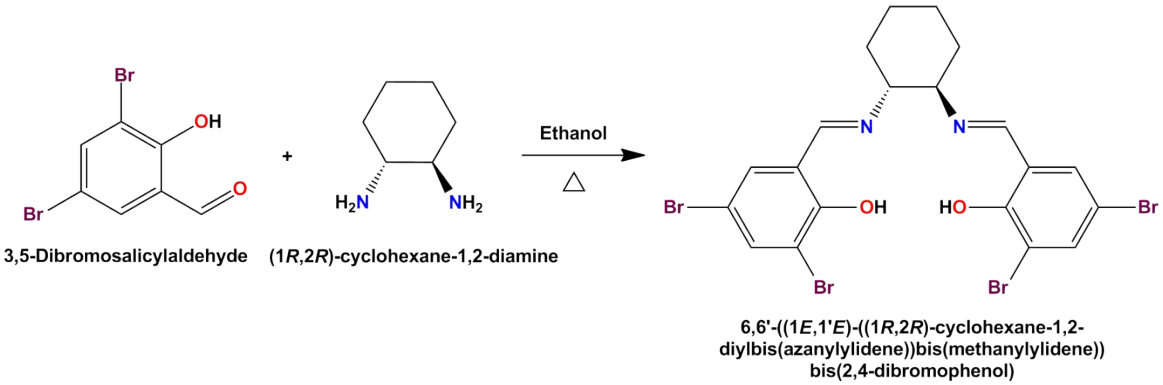

Scheme S1. Synthetic scheme for H_2L

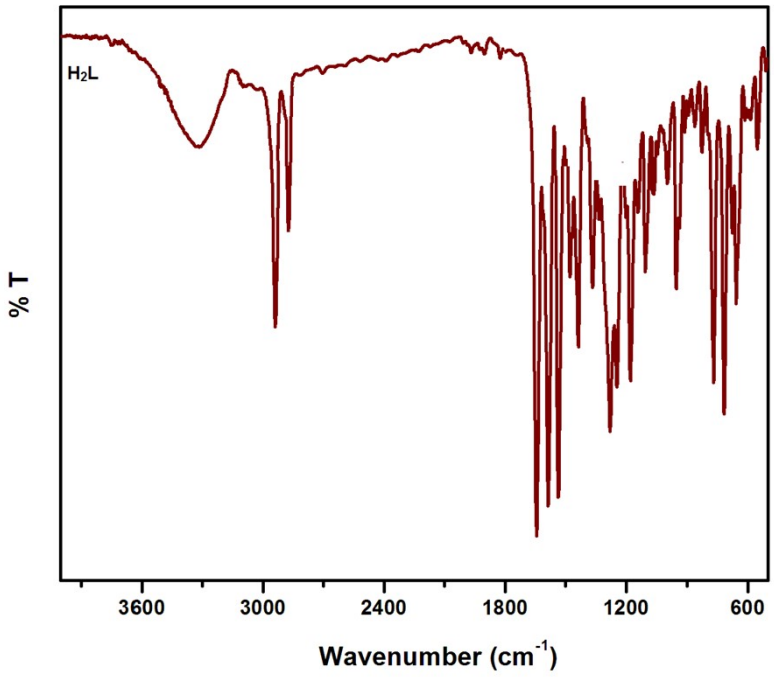

Fig. S1. FT-IR spectrum of H_2L

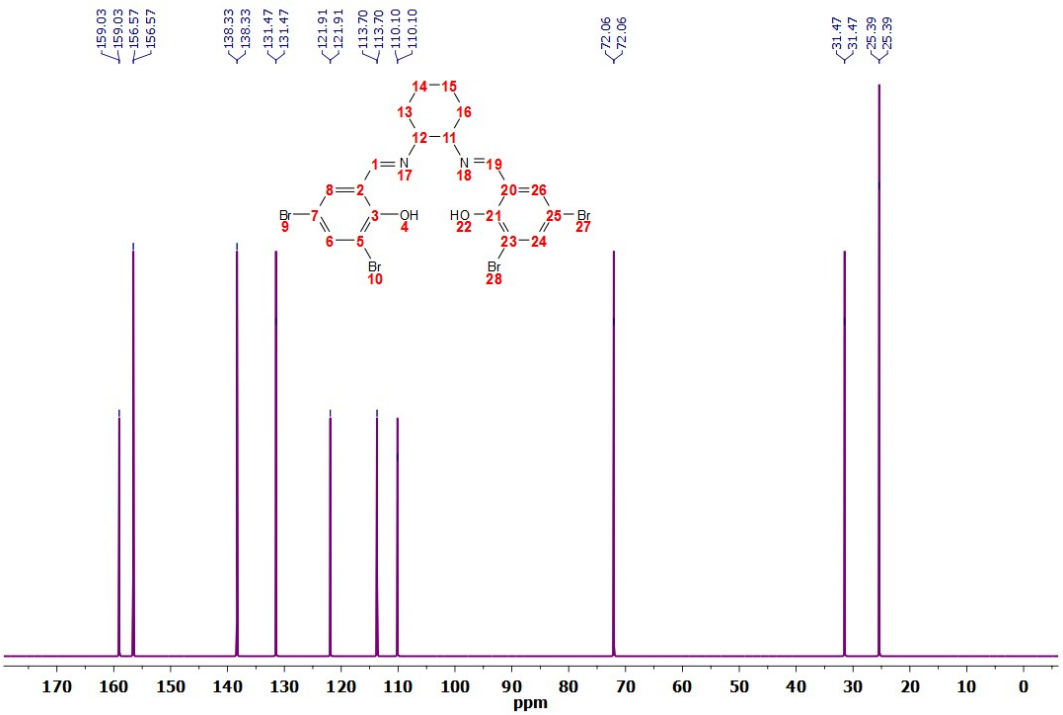

Fig. S2.^{13}C NMR spectrum of H_2L

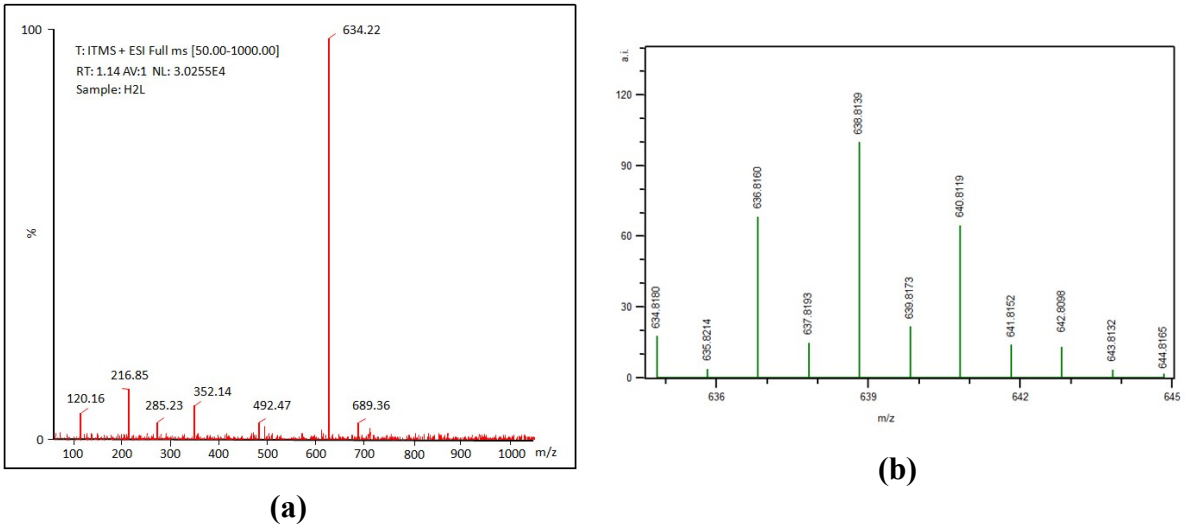

(a) **(b)**

Fig. S3. ESI-mass spectra of H_2L, **(a)** experimental; **(b)** simulated

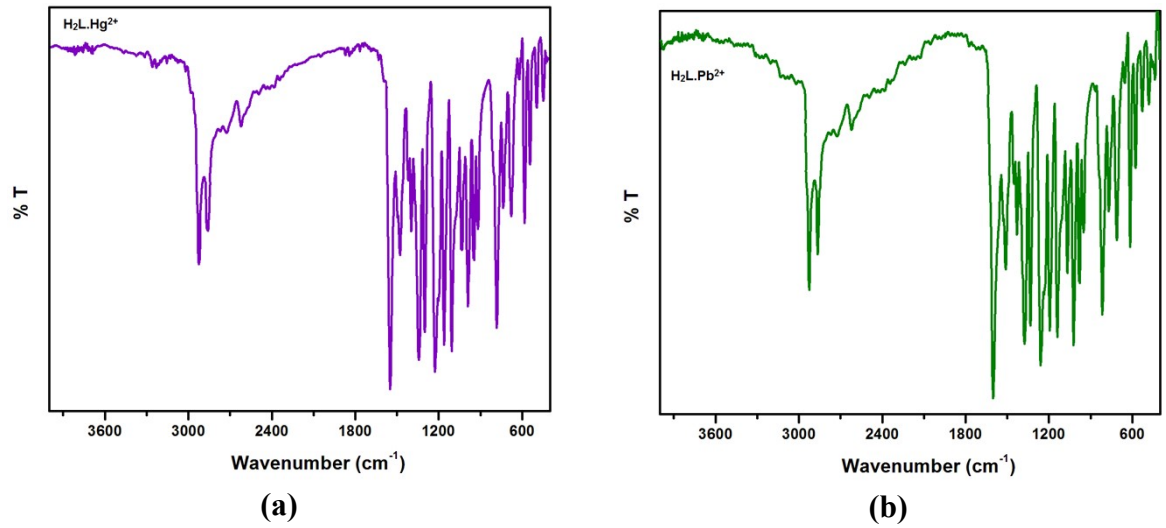

Fig. S4. FT-IR spectra of **(a)** $H_2L.Hg^{2+}$; **(b)** $H_2L.Pb^{2+}$

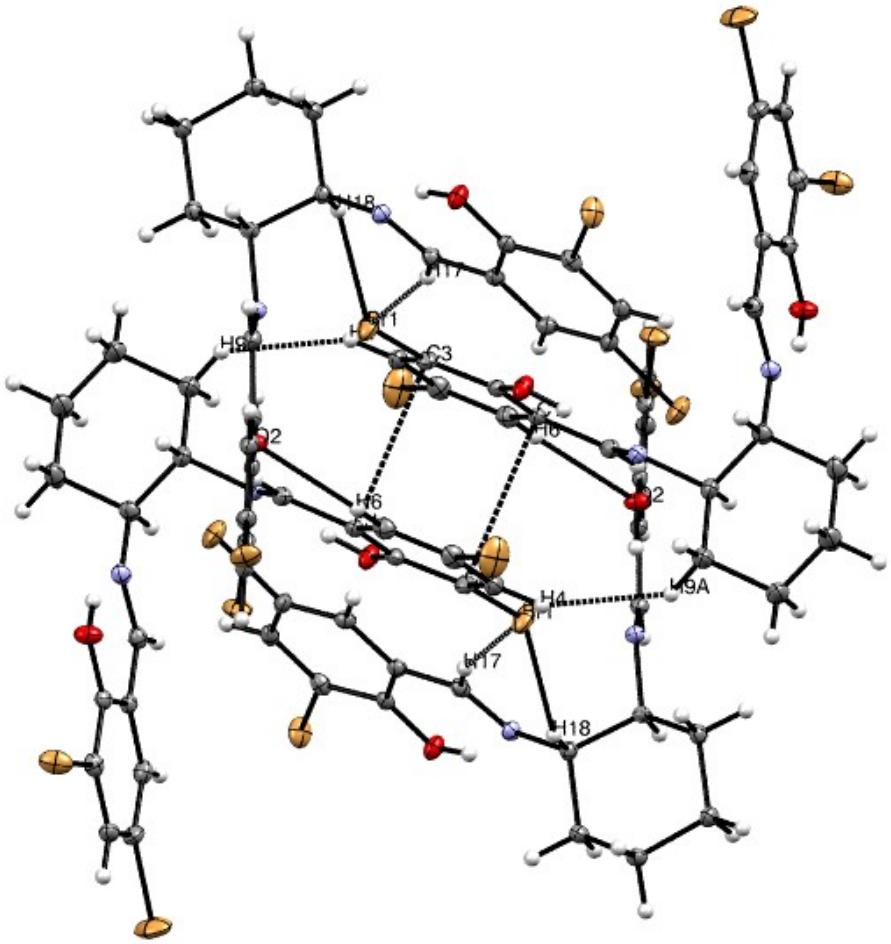

Fig. S5. 2D-coordination polymeric chain of H_2L

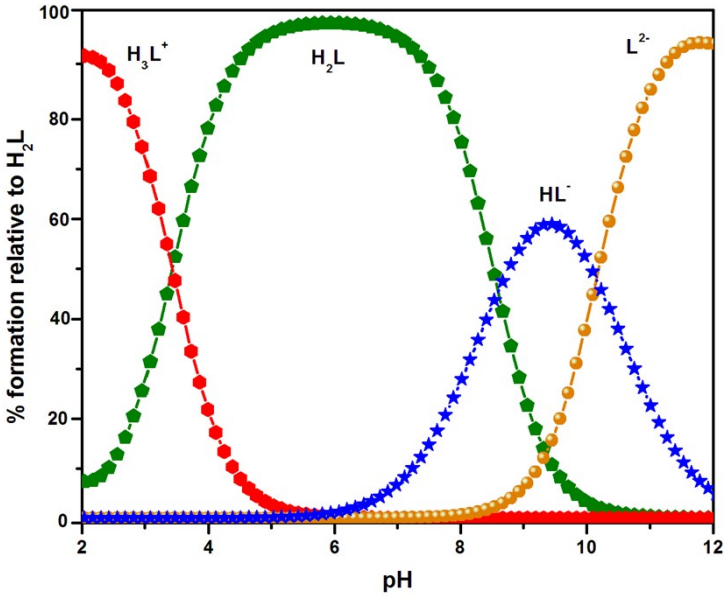

Fig. S6. Protonation equilibria diagram of H_2L

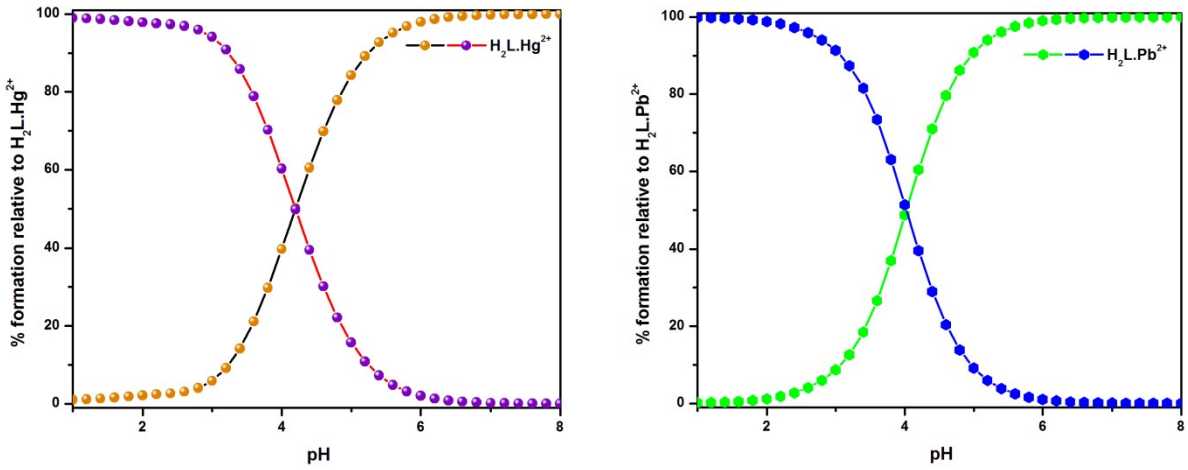

Fig. S7. Species distribution diagram of (a) $H_2L.Hg^{2+}$ and (b) $H_2L.Pb^{2+}$ equilibria in methanol/HEPES buffer (5 mM, pH 7.2; 1:9 v/v)

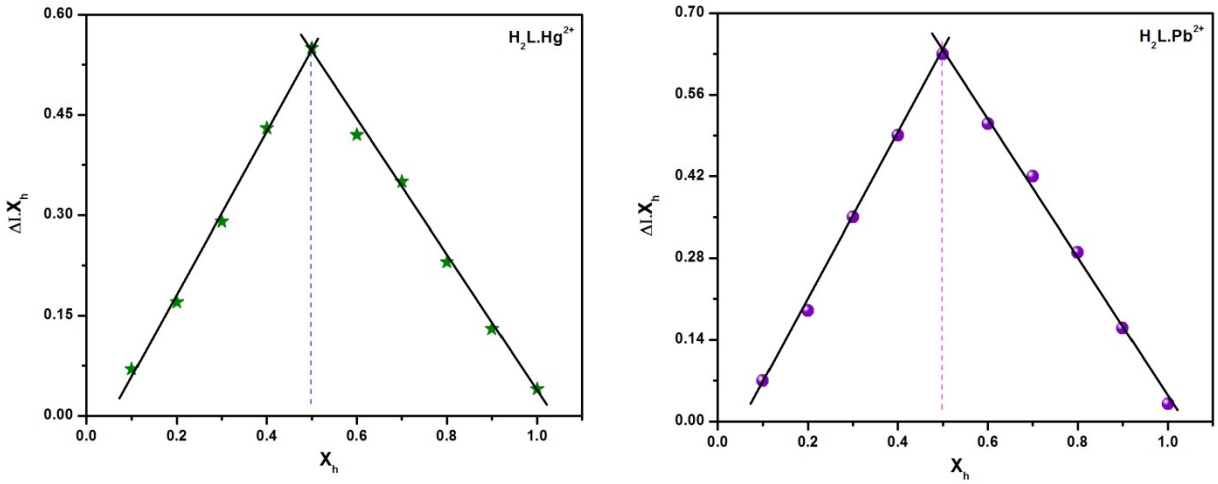

(a) **(b)**

Fig. S8. Job's plot analysis H_2L with **(a)** Hg^{2+} and **(b)** Pb^{2+}

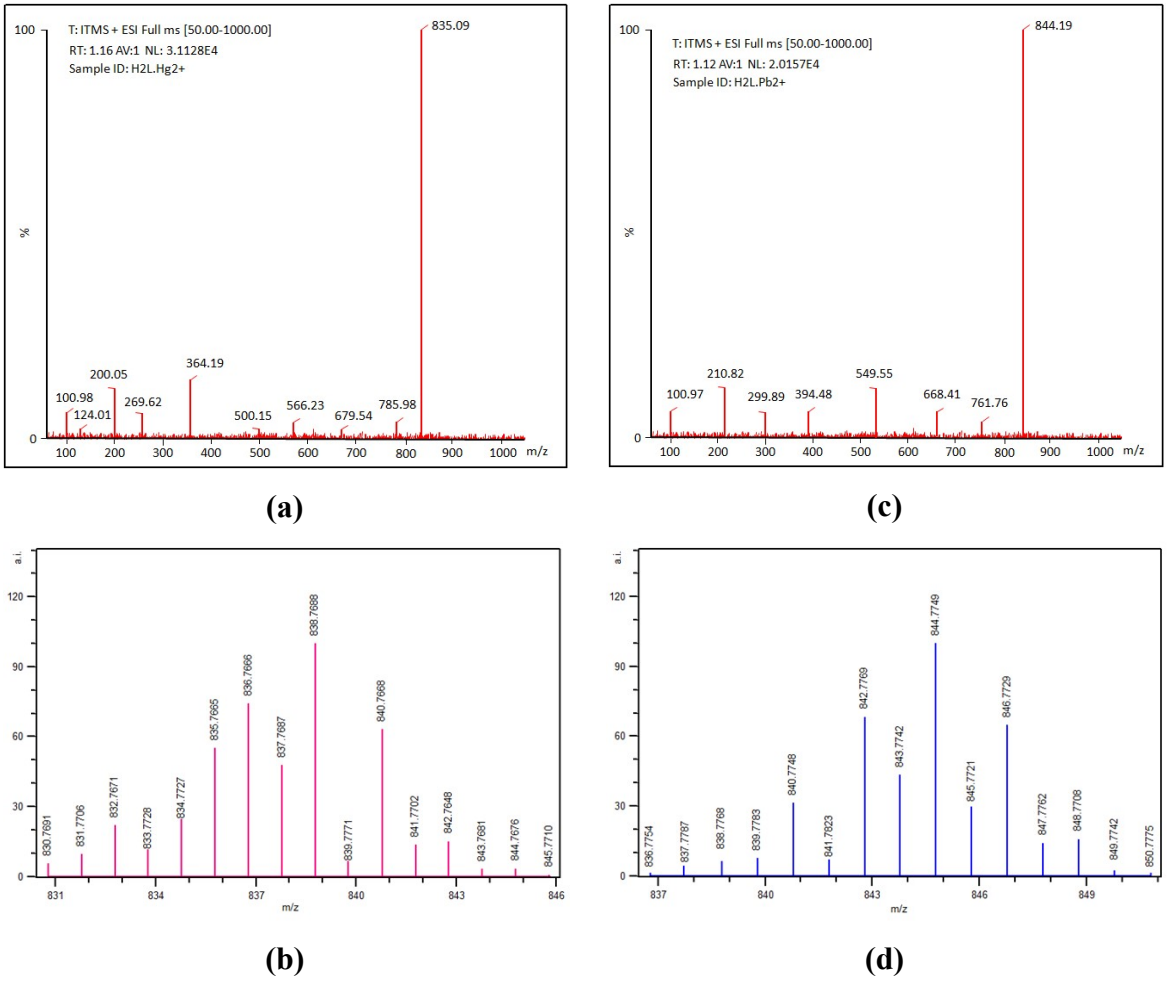

Fig. S9. ESI-mass spectra of **(a)** experimental $H_2L.Hg^{2+}$; **(b)** simulated $H_2L.Hg^{2+}$; **(c)** experimental $H_2L.Pb^{2+}$ and **(d)** simulated $H_2L.Pb^{2+}$

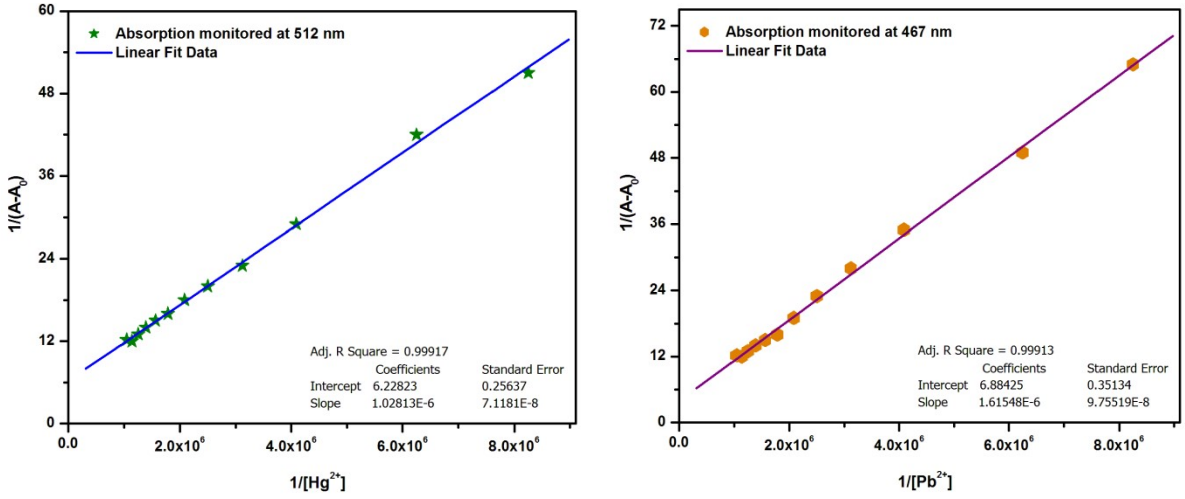

(a) **(b)**

Fig. S10. B-H plot from UV-vis titration data of with **(a)** Hg^{2+} and **(b)** Pb^{2+} concentration

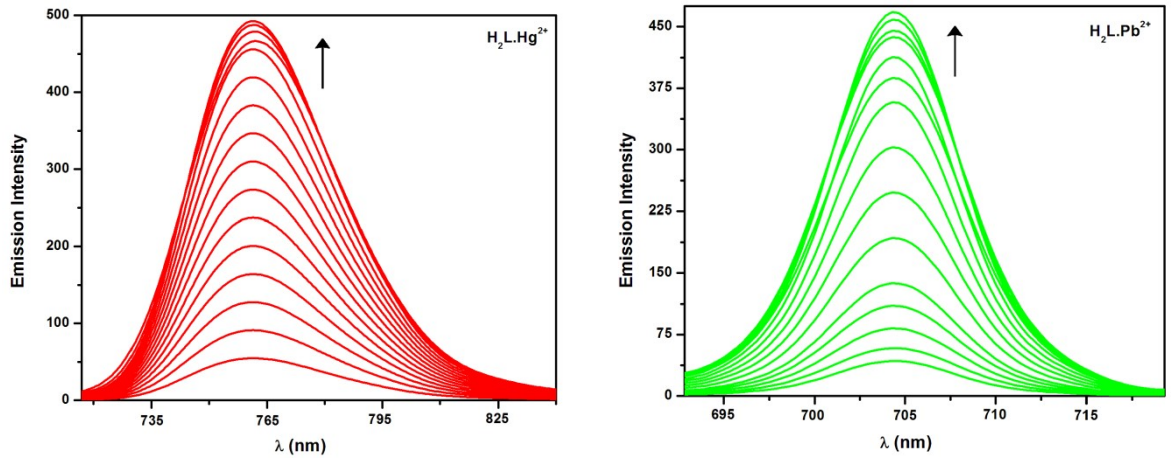

(a) **(b)**

Fig. S11. Fluorescence spectra of H_2L (10 μM) upon incremental addition of (a) Hg^{2+} (0.0 - 5.0 equiv.) and (b) Pb^{2+} (0.0 - 5.0 equiv.) in methanol/HEPES buffer (5 mM, pH 7.2; 1:9 v/v)

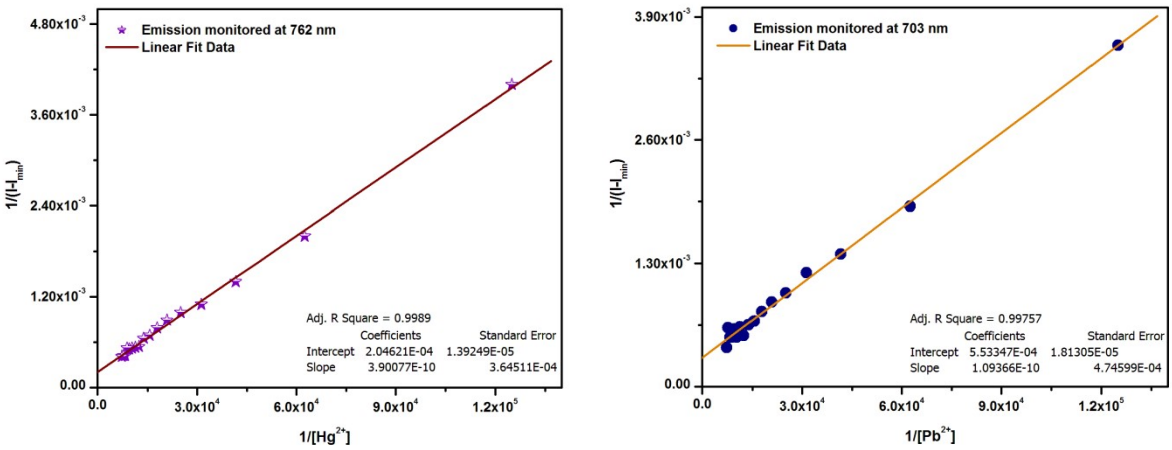

(a) **(b)**

Fig. S12. B-H plot from fluorescence titration data of with **(a)** Hg^{2+} and **(b)** Pb^{2+} concentration

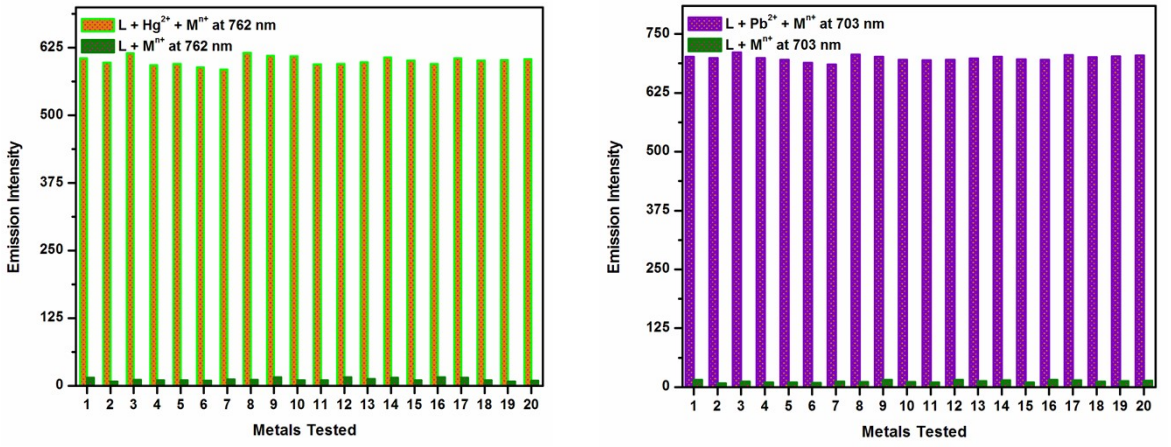

(a) **(b)**

Fig. S13. Fluorescence intensity of H_2L (10 μM) with (a) Hg^{2+} and (b) Pb^{2+} in the presence of other metal ions in methanol/HEPES buffer (5 mM, pH 7.2; 1:9 v/v) at room temperature

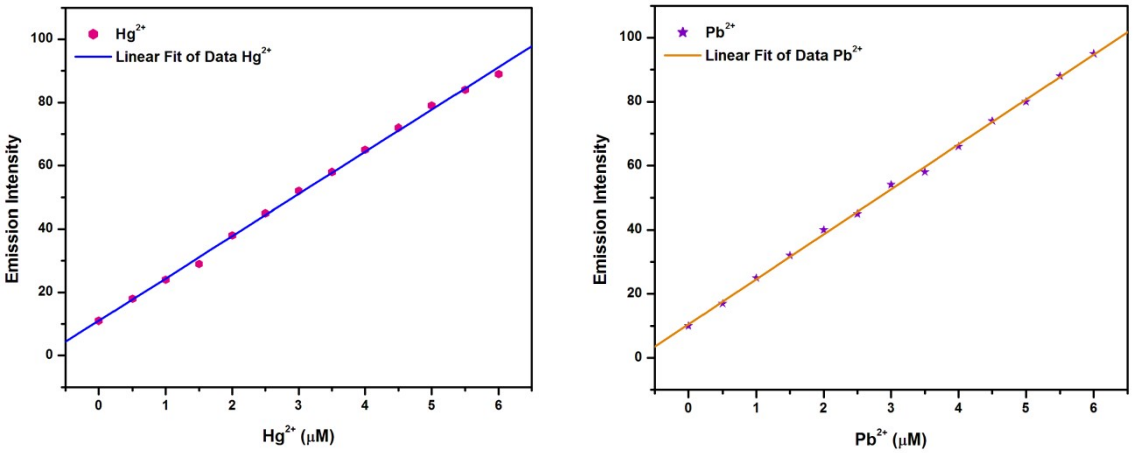

(a) **(b)**

Fig. S14. **(a)** Linear dynamic plot of fluorescence intensity (at 762 nm) vs. [Hg^{2+}] for the determination of S (slope) and **(b)** Linear dynamic plot of fluorescence intensity (at 703 nm) vs. [Pb^{2+}] for the determination of S (slope); [H_2L] = 10 μM

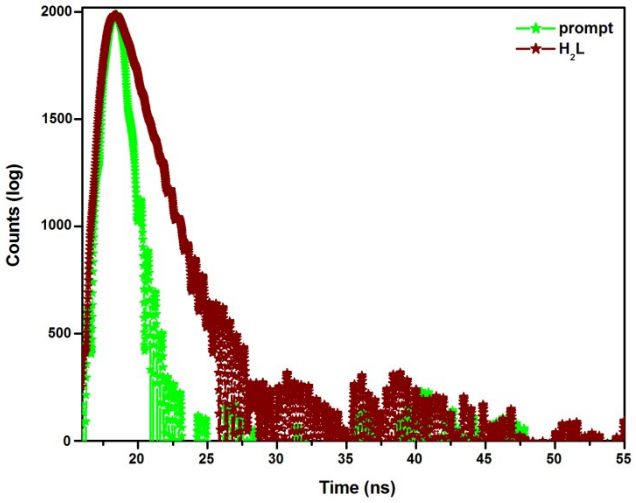

Fig. S15. Lifetime emission decay of H_2L (10 μM) in methanol/HEPES buffer (5 mM, pH 7.2; 1:9 v/v)

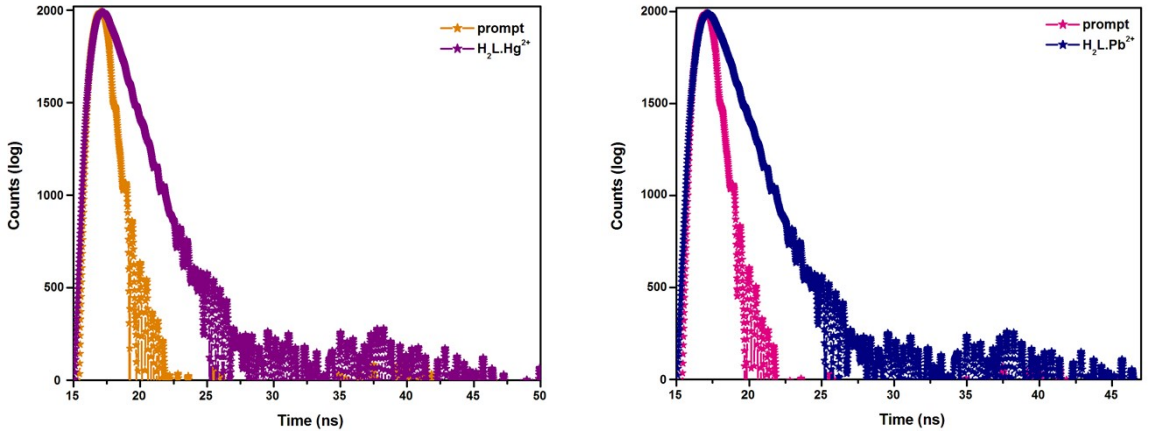

(a) **(b)**

Fig. S16. Lifetime emission decay of **(a)** $H_2L.Hg^{2+}$ and **(b)** $H_2L.Pb^{2+}$ in methanol/HEPES buffer (5 mM, pH 7.2; 1:9 v/v)

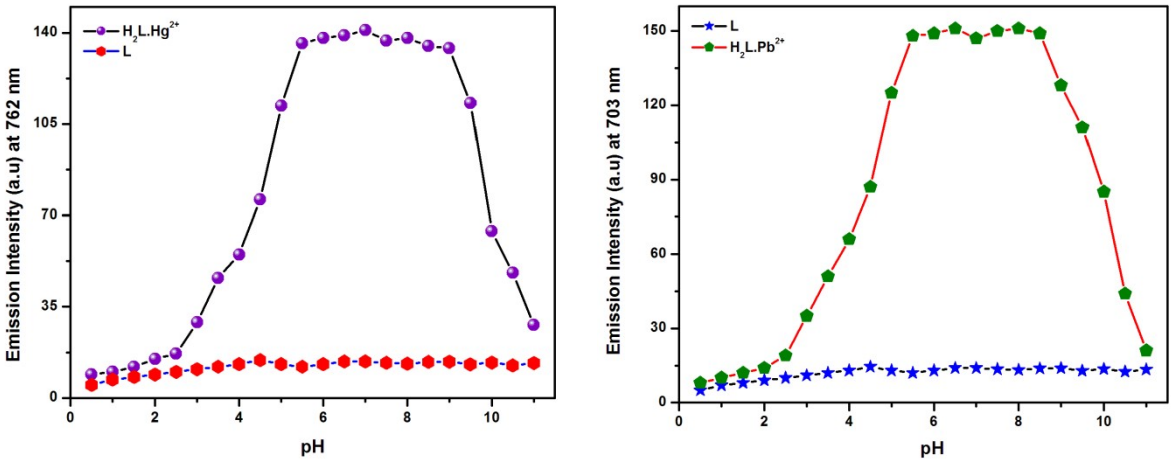

(a) **(b)**

Fig. S17. Fluorescence intensity of H_2L in the presence of **(a)** Hg^{2+} (λ_{em} = 600 nm; λ_{ex} = 762 nm); **(b)** Pb^{2+} (λ_{em} = 575 nm; λ_{ex} = 703 nm) at various pH values in methanol/HEPES buffer (5 mM, pH 7.2; 1:9 v/v)

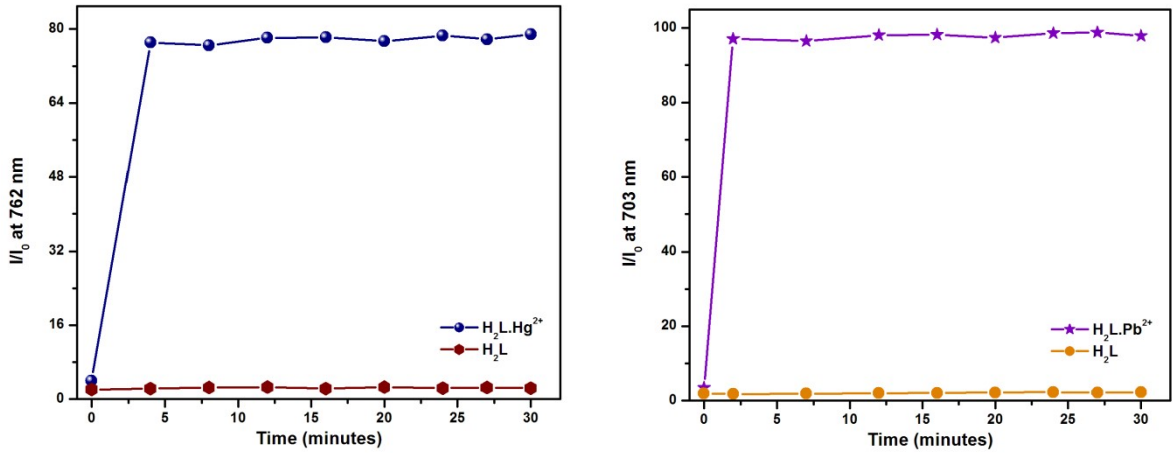

(a) **(b)**

Fig. S18. Emission intensity of **(a)** $H_2L.Hg^{2+}$; **(b)** $H_2L.Pb^{2+}$ as a function of time (0-30 minutes)

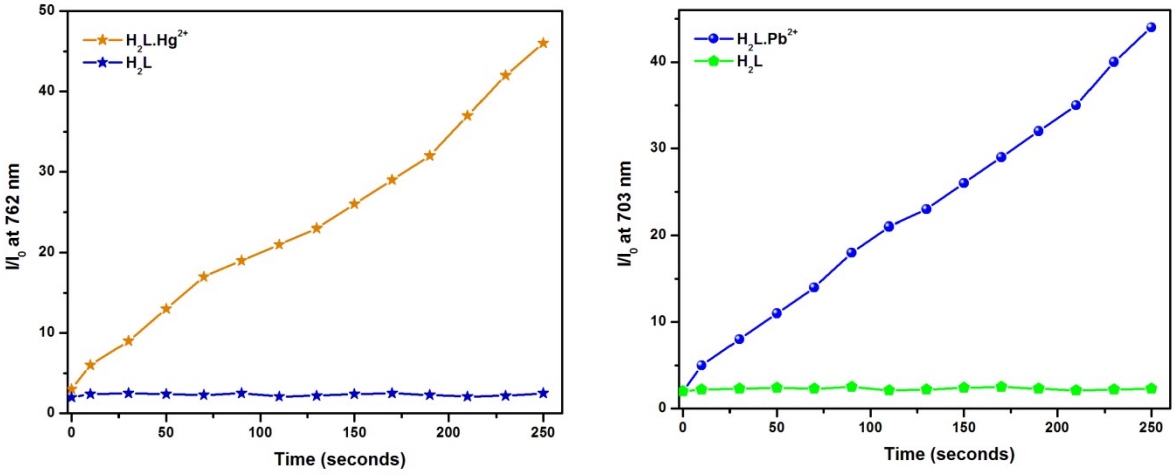

(a) **(b)**

Fig. S19. Fluorescence intensity of **(a)** $H_2L.Hg^{2+}$; **(b)** $H_2L.Pb^{2+}$ as a function of time (seconds)

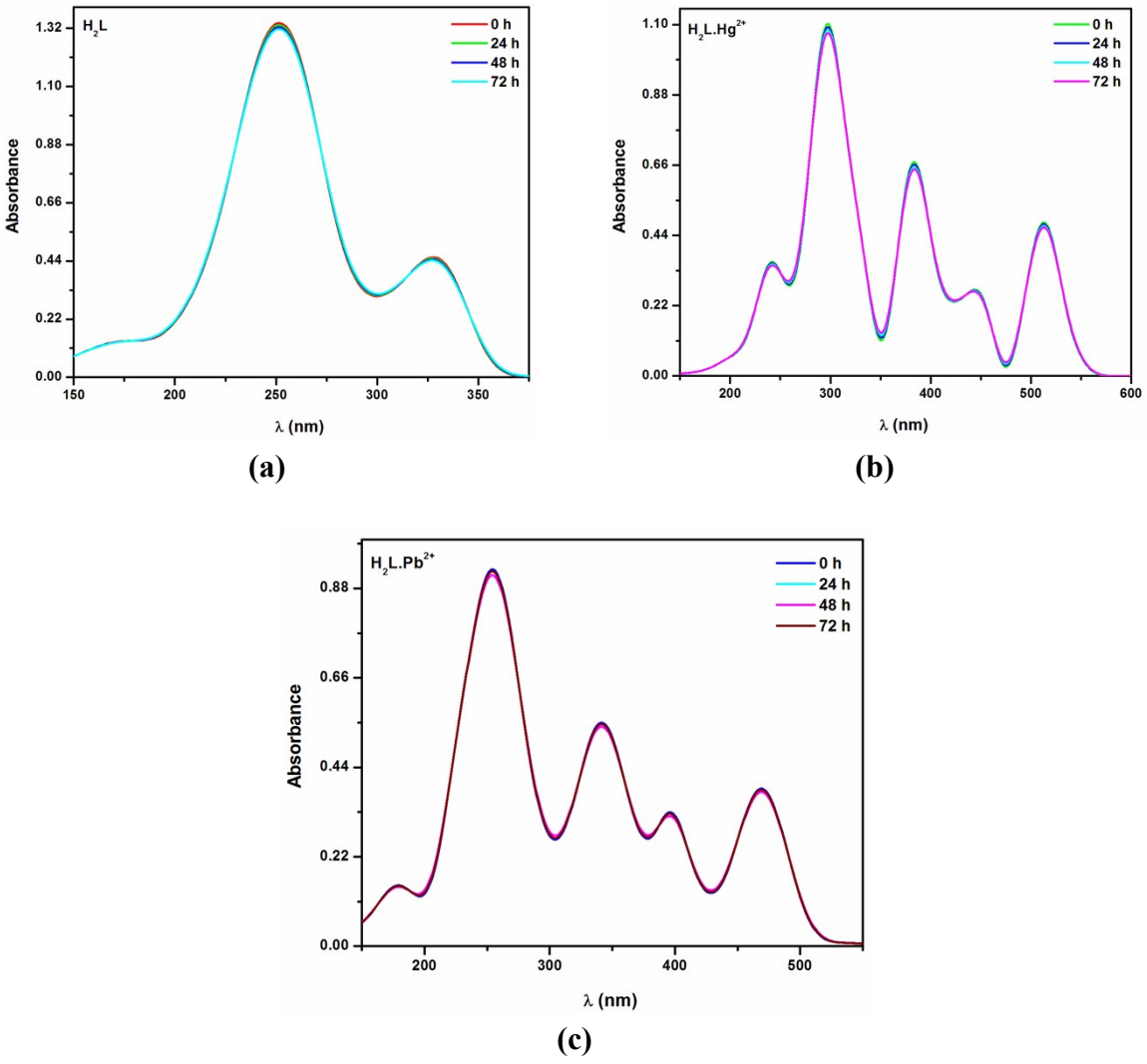

Fig. S20. Photostability tests of (a) H_2L, (b) $H_2L.Hg^{2+}$ and (c) $H_2L.Pb^{2+}$ measured by absorption spectroscopy in methanol/HEPES buffer (5 mM, pH 7.2, 1:9 v/v).

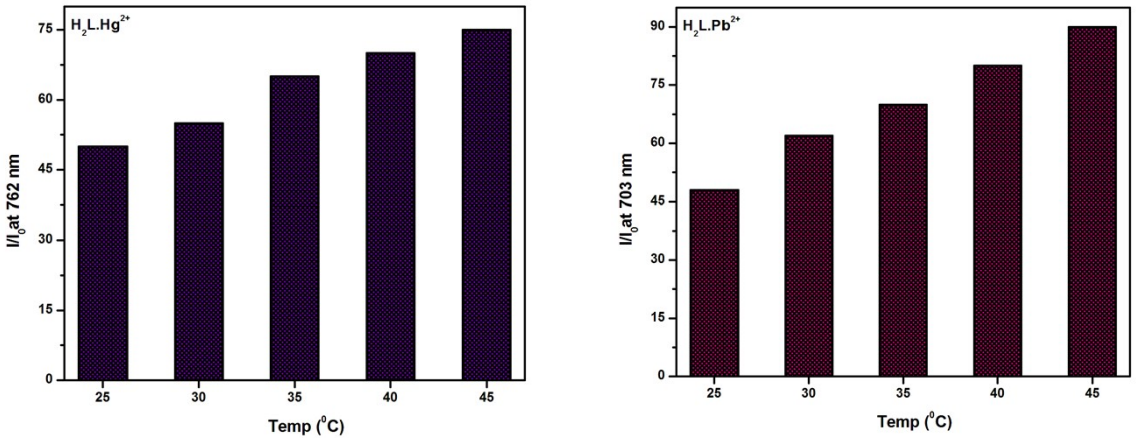

(a) **(b)**

Fig. S21. Fluorescence spectral changes of **(a)** $H_2L.Hg^{2+}$; **(b)** $H_2L.Pb^{2+}$ as a function of temperature (25-45˚C)

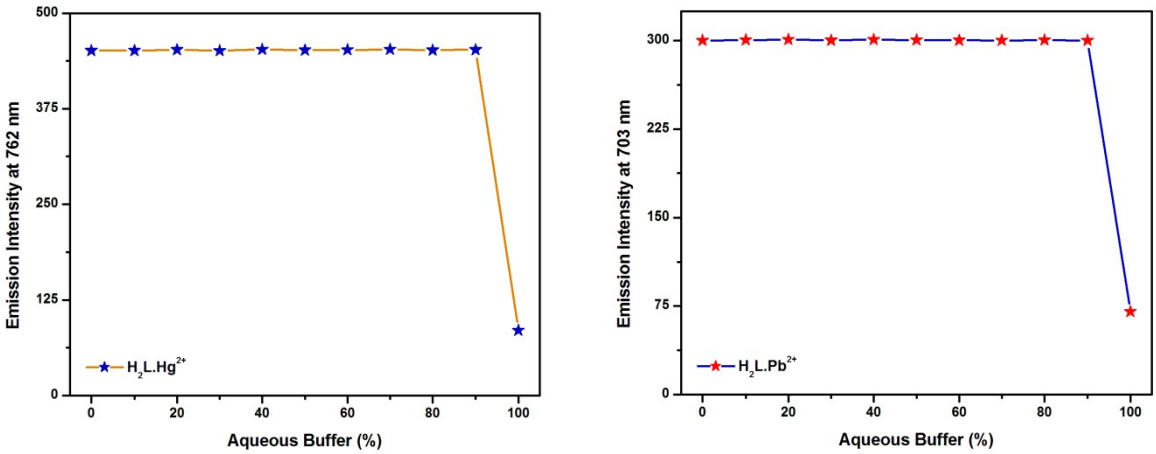

Fig. S22. Emission intensity of **(a)** $H_2L.Hg^{2+}$; **(b)** $H_2L.Pb^{2+}$ as a function of aqueous buffer concentration (0-99%)

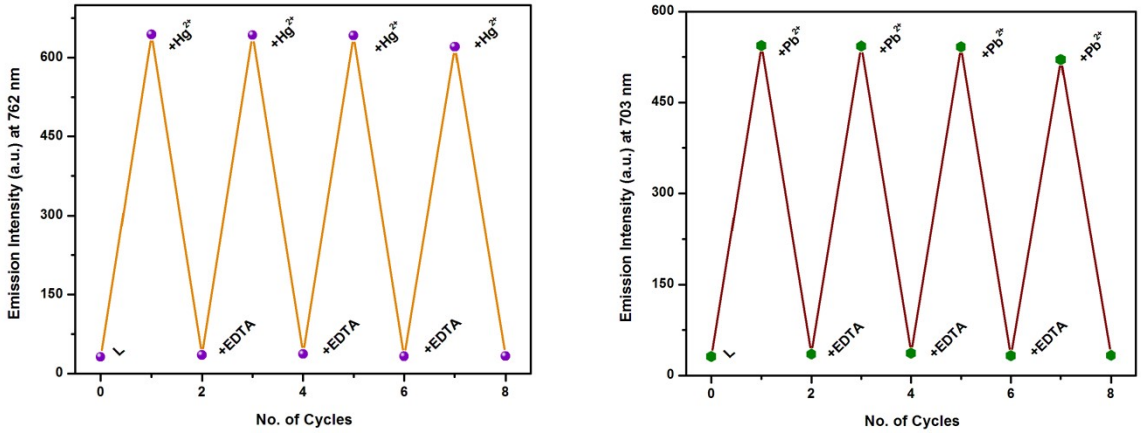

(a) **(b)**

Fig. S23. (a) Fluorescence intensities of $H_2L.Hg^{2+}$ (1:1) in the presence of EDTA for many cycles (λ_{ex} = 600 nm; λ_{em} = 762 nm); (b) Fluorescence intensities of $H_2L.Pb^{2+}$ (1:1) in the presence of EDTA for many cycles (λ_{ex} = 575 nm; λ_{em} = 703 nm)

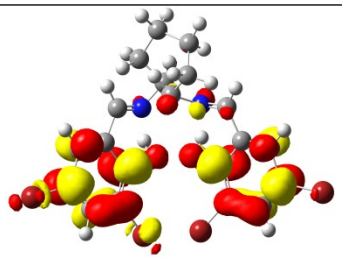	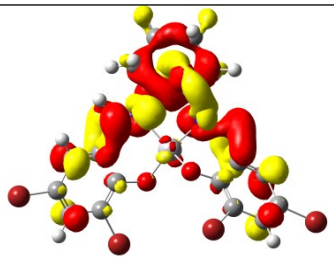	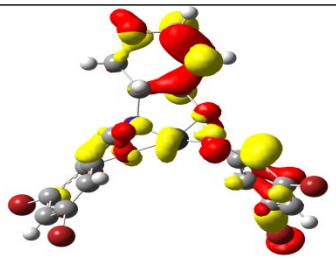
LUMO = -3.9658 (eV)	LUMO = -2.7254 (eV)	LUMO = -2.6048 (eV)
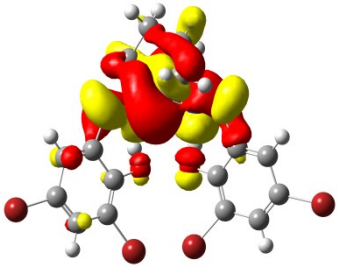	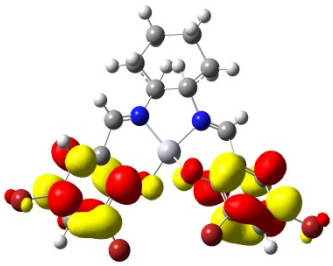	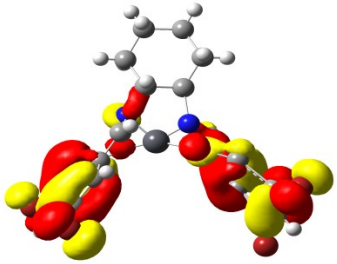
HOMO = -6.8114 (eV)	HOMO = -4.5406 (eV)	HOMO = -4.6632 (eV)
ΔE = 2.8456 (eV)	ΔE = 1.8152 (eV)	ΔE = 2.0584 (eV)
(a)	**(b)**	**(c)**

Fig. S24. FMO diagrams of **(a)** H_2L; **(b)** $H_2L.Hg^{2+}$ and **(c)** $H_2L.Pb^{2+}$ with energy gap as calculated from the DFT method

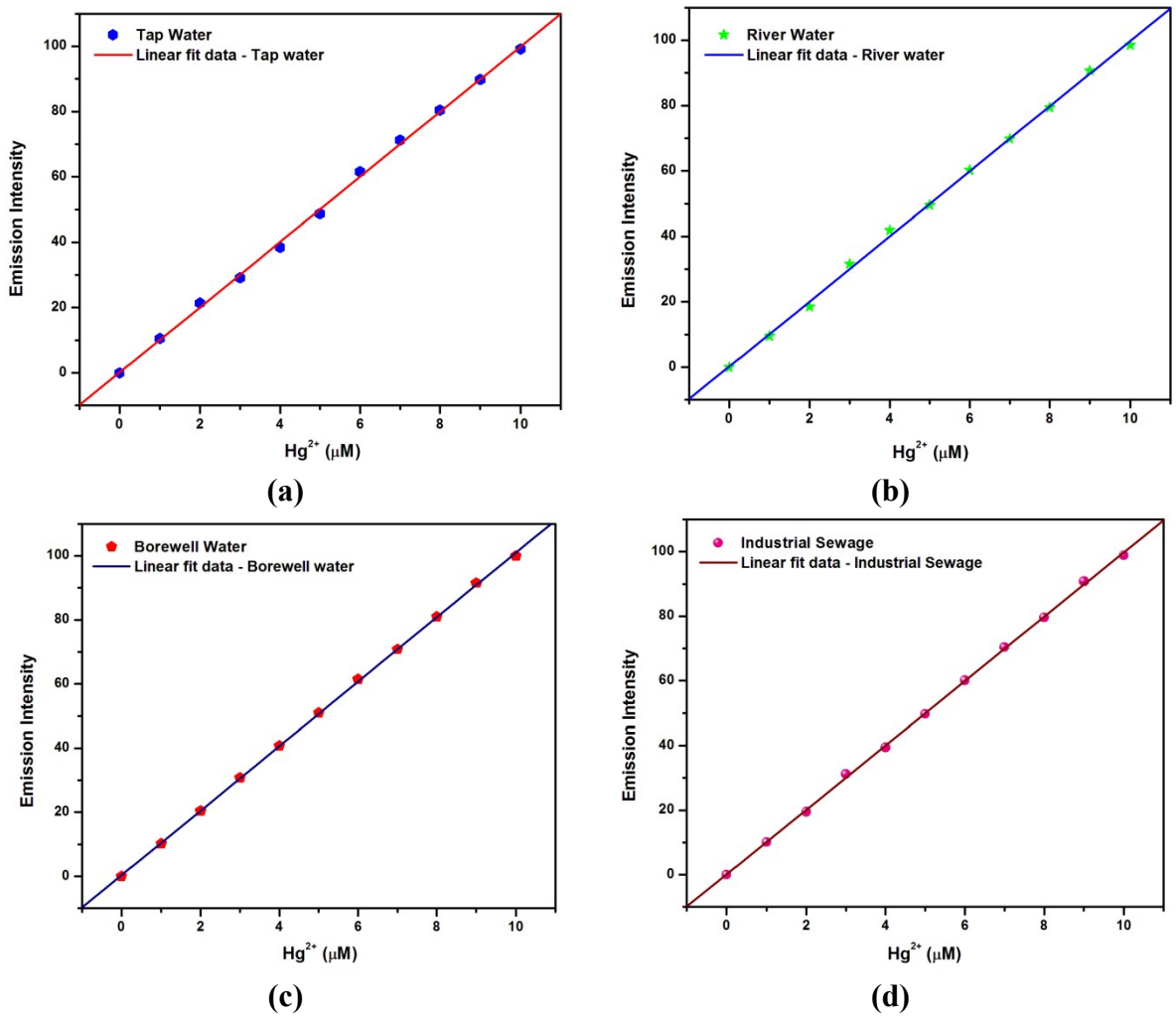

Fig. S25. Calibration sensitivity plot of H_2L for Hg^{2+}; (a) Tap water; (b) River water; (c) Bore well water and (d) Industrial sewage water

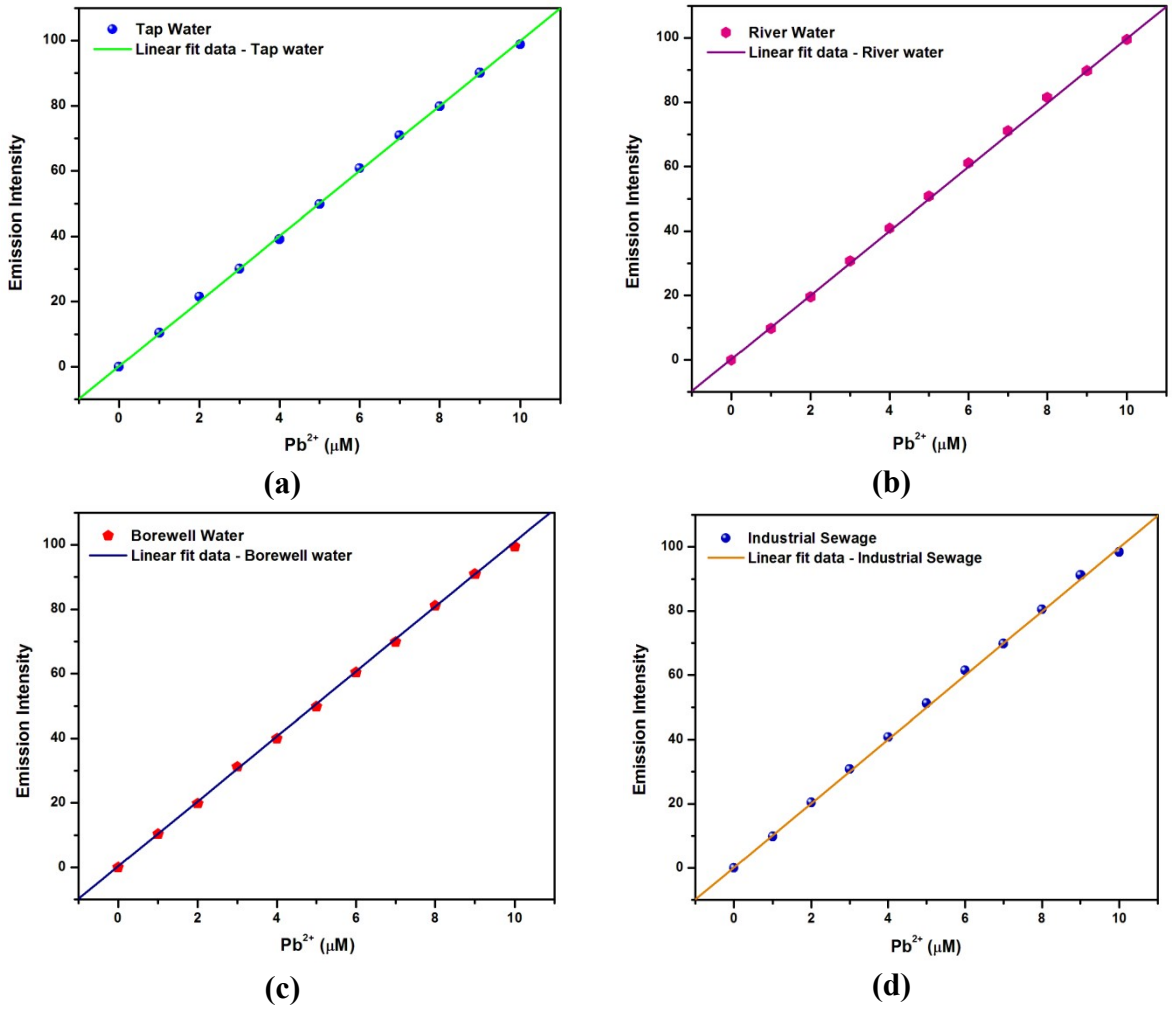

Fig. S26. Calibration sensitivity plot of H_2L for Pb^{2+}; (a) Tap water; (b) River water; (c) Bore well water and (d) Industrial sewage water

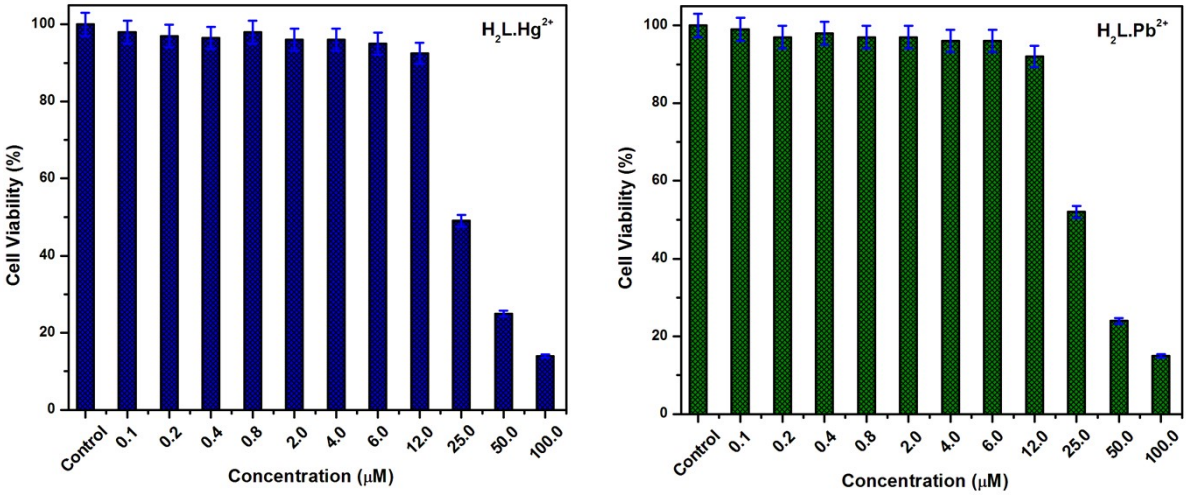

Fig. S27. MTT assay of (a) $H_2L.Hg^{2+}$ and (b) $H_2L.Pb^{2+}$ complex in the HeLa cell line

(a) **(b)** **(c)** **(d)**

Fig. S28. Fluorescence bioimaging of HeLa cells; (a) control cells; (b) cells treated with 2 μM H_2L; (c) cells treated with 2 μM Hg^{2+}; (d) cells treated with 2 μM Hg^{2+} and H_2L.

(a) **(b)** **(c)** **(d)**

Fig. S29. Fluorescence bioimaging of HeLa cells; (a) control cells; (b) cells treated with 4 μM H_2L; (c) cells treated with 4 μM Hg^{2+}; (d) cells treated with 4 μM Hg^{2+} and H_2L.

(a) **(b)** **(c)** **(d)**

Fig. S30. Fluorescence bioimaging of HeLa cells; (a) control cells; (b) cells treated with 2 μM H_2L; (c) cells treated with 2 μM Pb^{2+}; (d) cells treated with 2 μM Pb^{2+} and H_2L.

(a) **(b)** **(c)** **(d)**

Fig. S31. Fluorescence bioimaging of HeLa cells; (a) control cells; (b) cells treated with 4 μM H_2L; (c) cells treated with 4 μM Pb^{2+}; (d) cells treated with 4 μM Pb^{2+} and H_2L.

(a) **(b)** **(c)** **(d)**

Fig. S32. Fluorescence images of HeLa cells with 1 μM propidium iodide; (a) control cells; (b) cells treated with 2 μM H_2L; (c) cells treated with 2 μM Hg^{2+}; (d) cells treated with 2 μM Hg^{2+} and H_2L.

(a) **(b)** **(c)** **(d)**

Fig. S33. Fluorescence images of HeLa cells with 1 μM propidium iodide; (a) control cells; (b) cells treated with 4 μM H_2L; (c) cells treated with 4 μM Hg^{2+}; (d) cells treated with 4 μM Hg^{2+} and H_2L.

(a) **(b)** **(c)** **(d)**

Fig. S34. Fluorescence images of HeLa cells with 1 μM propidium iodide; (a) control cells; (b) cells treated with 2 μM H_2L; (c) cells treated with 2 μM Pb^{2+}; (d) cells treated with 2 μM Pb^{2+} and H_2L.

(a) **(b)** **(c)** **(d)**

Fig. S35. Fluorescence images of HeLa cells with 1 μM propidium iodide; (a) control cells; (b) cells treated with 4 μM H_2L; (c) cells treated with 4 μM Pb^{2+}; (d) cells treated with 4 μM Pb^{2+} and H_2L.

Binding of H_2L with Hg^{2+}/Pb^{2+} by UV-vis Method

The $H_2L.Hg^{2+}/Pb^{2+}$ binding constant was calculated using the Benesi-Hildebrand (B-H) plot.[S1-S3]

$$1/(A - A_0) = a/(a - b)\{1/K_a[M] + 1 \text{ ……(1)}$$

where A_0 is absorbance of free H_2L, A is absorbance of H_2L with Hg^{2+}/Pb^{2+} ions, K_a is the binding constant (M^{-1}) and [M] is the concentration of Hg^{2+}/Pb^{2+} ions added during titration. The association constant (K_a) could be determined from the slope of the straight line of the plot of $1/(A - A_0)$ vs. $[1/M^{II}]$.

Binding of H_2L with Hg^{2+}/Pb^{2+} by Emission Method

In addition the binding constant value of Hg^{2+}/Pb^{2+} ions with H_2L has been examined by emission spectroscopic method using the modified Benesi-Hildebrand equation,

$$1/(I - I_0) = 1/\{K(I_{max} - I_0)C\}+1/(I_{max} - I_0) \text{ ……(2)}$$

where I_0 is the emission intensity of H_2L in the absence of Hg^{2+}/Pb^{2+} ions, I is the observed fluorescence intensity at that particular wavelength in the presence of a certain concentration of the Hg^{2+}/Pb^{2+} (C), I_{max} is the maximum emission intensity value that was obtained during the titration with varying Hg^{2+}/Pb^{2+} concentration, K is the binding constant (M^{-1}) and was determined from the slope of the linear plot and C is the concentration of the Hg^{2+}/Pb^{2+} ions added during titration.

Job Plot Technique

The methanol/HEPES buffer (5 mM, pH 7.2; 1:9v/v) was used to dissolve the H_2L (0.01M). 5.0 ml bottles were filled with 100, 90, 80, 70, 60, 50, 40, 30, 20, 10, and 0 μL of the H_2L solution. Each bottle received water until its total content reached 4.0 ml. Water was used to dissolve Hg^{2+}/Pb^{2+} ions (0.01M). Each diluted solution of H_2L was mixed with 0, 10, 20, 30, 40, 50, 60, 70, 80, 90, and 100 μL of the Hg^{2+}/Pb^{2+} ion solution. The total volume of each bottle was 5.0 ml. Absorption spectra were recorded at room temperature following a 5 min shake. Job's plots were drawn by plotting $\Delta I.X_h$ vs. X_h, where ΔI = change of absorbance at 512 nm (for Hg^{2+}) and 467 nm (for Pb^{2+}) during titration and X_h is the mole fraction of Hg^{2+}/Pb^{2+} ions).

pH Study

An automatic potentiometric titrator (HANNA-HI-902, USA) was used to perform the pH titrations at 310 K using a combination glass electrode (accuracy ± 0.01 pH unit). To calibrate the equipment, standard buffer solutions were used.[S4] Using $NaClO_4$ as the supporting electrolyte, the ionic strength of each solution was brought down to 0.10 M. Based on measurements of $[H^+]$, $[OH^-]$, and pH in many tests, the ion product of water ($K = [H^+][OH^-]$) at 0.10 M $NaClO_4$ in methanol/HEPES buffer (5 mM, pH 7.2; 1:9 v/v) combination was determined. The solution was bubbled with nitrogen gas both before to and throughout the titrations. There were several titrations performed for every system. From its solutions of concentrations ranging from 1.0×10^{-3} to 3.0×10^{-3} M, the dissociation constants (p*K*a) of H_2L were determined. The MINIQUAD-75 program was used to calculate the pKa values. Using HYSS, the concentration distribution profiles were acquired.[S5]

Quantum Yield Calculation

Quantum yield (Φ_x) for H_2L and $H_2L.Hg^{2+}/Pb^{2+}$ was calculated using standard solutions of fluorescein $(\Phi_x = 0.79)$ in methanol at an excitation wavelength 441 nm. The quantum yield was determined by the following eqn,

$$\Phi_x = \Phi_{st} \bullet (A_{st}/A_x) \bullet (F_x/F_{st}) \bullet (n_x^2/n_{st}^2) \bullet (D_x/D_{st})$$

Where,

Φ_x - Quantum yield of the sample

Φ_{st} - Quantum yield of the reference

A_x, A_{st} - Absorbance of the sample and the reference

F_x , F_{st} - Areas of emission for the sample and the reference

n_x^2 , n_{st}^2 - Refractive indexes of the solvents

D_x , D_{st} - Dilution factor of the sample and reference, respectively

Calculation:

For Hg^{2+}

$\Phi_{st} = 0.79$, $A_{st} = 441$ nm, $A_x = 512$ nm, $F_x = 64025.8$, $F_{st} = 109921.3$, $(n) = 1.3335$, $D_x = 0.002$ and $D_{st} = 0.003$

$\Phi_x = 0.79 \bullet (441/512) \bullet (64025.8/109921.3) \bullet (1.3335/1.3335) \bullet (0.002/0.003)$

$\Phi_x = 0.68045 \bullet (64025.8/109921.3) \bullet 1 \bullet 0.66667$

$\Phi_x = 0.45363 \bullet (64025.8/109921.3)$

$$\Phi_x = 0.2642$$

For Pb^{II}

$\Phi_{st} = 0.79$, $A_{st} = 441$ nm, $A_x = 467$ nm, $F_x = 64098.2$, $F_{st} = 128456.8$, $(n) = 1.3335$, $D_x = 0.002$ and $D_{st} = 0.003$

$$\Phi_x = 0.79 \bullet (441/467) \bullet (64098.2/128456.8) \bullet (1.3335/1.3335) \bullet (0.002/0.003)$$

$$\Phi_x = 0.74602 \bullet (64098.2/128456.8) \bullet 1 \bullet 0.66667$$

$$\Phi_x = 0.49737 \bullet (64098.2/128456.8)$$

$$\Phi_x = 0.2132$$

For H_2L

$\Phi_{st} = 0.79$, $A_{st} = 441$ nm, $A_x = 332$ nm, $F_x = 25122.7$, $F_{st} = 189874.8$, $(n) = 1.3252$, $D_x = 0.002$ and $D_{st} = 0.003$

$$\Phi_x = 0.79 \bullet (441/332) \bullet (25748.9/179799.5) \bullet (1.3252/1.3252) \bullet (0.002/0.003)$$

$$\Phi_x = 0.74602 \bullet (25748.9/179799.5) \bullet 1 \bullet 0.66667$$

$$\Phi_x = 0.69961 \bullet (25748.9/259799.5)$$

$$\Phi_x = 0.0693$$

Reversibility Studies

EDTA disodium salt has demonstrated the reversible capability of the proposed sensor. Methanol (1.0 mL) was used to dissolve the H_2L (10 μM), and 1.0 mL of H_2L solution was combined with 4.0 ml of the Hg^{2+}/Pb^{2+} solution. After dissolving 0.5 mmol of EDTA in 5.0 ml of water, 2.0 mL of the EDTA solution was added to the $H_2L.Hg^{2+}/Pb^{2+}$ solution. Fluorescence spectra were recorded at room temperature after two minutes of mixing. The emission intensity of the $H_2L.Hg^{2+}/Pb^{2+}$ is quenched by the disodium salt of EDTA, a heavy metal ion chelator, suggesting that H_2L reversibly coordinates to metal ions.

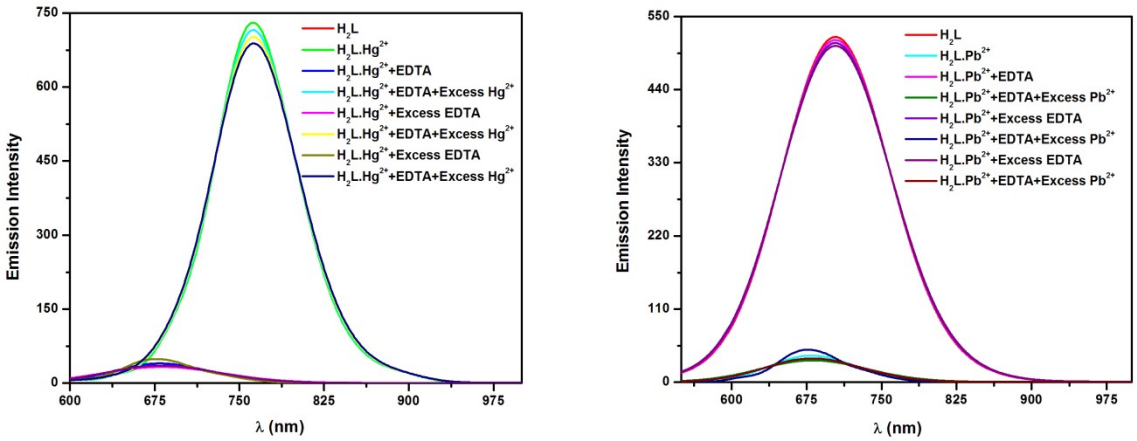

(a) **(b)**

Fig. S36. Fluorescence changes of H_2L (10 μM) after the addition of (a) Hg^{2+}; (b) Pb^{2+} and EDTA (1 equiv.) in methanol/HEPES buffer (5 mM, pH 7.2, 1:9 v/v)

Table S1 Bond lengths [Å] for H_2L

Bond lengths [Å]	
Br(1)-C(3)	1.8882(18)
Br(2)-C(5)	1.8929(18)
O(1)-H(1)	0.8400
O(1)-C(2)	1.341(2)
N(1)-C(8)	1.462(2)
N(1)-C(7)	1.276(2)
C(8)-C(8)#1	1.533(3)
C(8)-C(9)	1.528(3)
C(9)-C(10)	1.523(3)
C(10)-C(10)#1	1.523(4)
Br(3)-C(13)	1.8911(17)
Br(4)-C(15)	1.8985(17)
O(2)-H(2)	0.8400
O(2)-C(12)	1.341(2)
N(2)-C(17)	1.281(2)
N(2)-C(18)	1.468(2)

Table S2 Bond angles [°] for H_2L

Bond angles [°]	
C(2)-O(1)-H(1	109.5
C(7)-N(1)-C(8)	118.58(15)
N(1)-C(8)-C(8)#1	108.95(12)
N(1)-C(8)-H(8)	109.2
N(1)-C(8)-C(9)	109.62(14)
N(1)-C(7)-H(7)	119.3
N(1)-C(7)-C(1)	121.44(16)
C(4)-C(3)-Br(1)	118.56(13)
C(2)-C(3)-Br(1)	119.42(13)
O(1)-C(2)-C(3)	120.19(16)
O(1)-C(2)-C(1)	122.22(15)
C(3)-C(2)-C(1)	117.59(16)
C(6)-C(5)-Br(2)	120.15(14)
C(6)-C(5)-C(4)	121.20(17)
C(4)-C(5)-Br(2)	118.65(14)
C(12)-O(2)-H(2)	109.5
C(17)-N(2)-C(18)	116.96(14)
C(16)-C(15)-Br(4)	120.09(14)
C(14)-C(15)-Br(4)	118.72(13)
N(2)-C(17)-C(11)	122.36(16)
N(2)-C(17)-H(17)	118.8
C(12)-C(13)-Br(3)	119.19(13)
C(14)-C(13)-Br(3)	119.07(13)
N(2)-C(18)-C(18)#2	111.83(11)
N(2)-C(18)-H(18)	108.9
N(2)-C(18)-C(19)	109.54(13)
O(2)-C(12)-C(11)	121.78(15)
O(2)-C(12)-C(13)	120.25(15)

Table S3 Torsion angles [°] for H_2L

Torsion angles [°]	
Br(1)-C(3)-C(2)-O(1)	2.4(2)
Br(1)-C(3)-C(2)-C(1)	-176.88(12)
N(1)-C(8)-C(9)-C(10)	176.38(16)
N(1)-C(7)-C(1)-C(6)	175.51(16)
N(1)-C(7)-C(1)-C(2)	-2.6(3)
C(8)-N(1)-C(7)-C(1)	-178.38(15)
C(6)-C(1)-C(2)-O(1)	-179.18(16)
C(4)-C(3)-C(2)-O(1)	-179.92(16)
C(7)-N(1)-C(8)-C(8)#1	-121.56(18)
C(7)-N(1)-C(8)-C(9)	117.33(18)
C(7)-C(1)-C(2)-O(1)	-1.1(2)
C(3)-C(4)-C(5)-Br(2)	-179.19(13)
C(1)-C(6)-C(5)-Br(2)	-179.95(13)
C(5)-C(4)-C(3)-Br(1)	176.65(13)
Br(3)-C(13)-C(12)-O(2)	-3.3(2)
Br(3)-C(13)-C(12)-C(11)	175.36(12)
Br(3)-C(13)-C(14)-C(15)	-176.18(13)
Br(4)-C(15)-C(16)-C(11)	177.50(12)
Br(4)-C(15)-C(14)-C(13)	-178.55(13)
N(2)-C(18)-C(19)-C(20)	177.75(14)
C(17)-N(2)-C(18)-C(18)#2	108.82(19)
C(17)-N(2)-C(18)-C(19)	-130.47(16)
C(17)-C(11)-C(12)-O(2)	3.9(2)
C(16)-C(11)-C(17)-N(2)	178.70(16)
C(16)-C(11)-C(12)-O(2)	179.66(15)
C(18)-N(2)-C(17)-C(11)	175.40(14)
C(12)-C(11)-C(17)-N(2)	-5.5(2)
C(14)-C(13)-C(12)-O(2)	179.24(15)

Symmetry transformations used to generate equivalent atoms: #1 -x+3/2,y,-z+3/2; #2 -x+3/2,y,-z+1/2

Table S4. Hydrogen bonds for H_2L (Å)

Atom1	Atom2	Length
H4	H9A	2.366
C3	C1	3.363
H6	O2	2.546
Br	H17	2.846
Br	H18	2.907

Table S5. Comparison of reported detection limit of Hg^{2+} and Pb^{2+} sensors with the present work.

S. No.	Compounds	Detection Limit	Ref.
1.	Cou-S	8.3 nM for Hg^{2+}; 10.5 nM for Pb^{2+}	S6
2.	TBA	5.0 nM for Hg^{2+}; 300 pM for Pb^{2+}	S7
3.	FNA	10.45 nM for Hg^{2+}; 2.65 nM for Pb^{2+}	S8
4.	RPU	7×10^{-9} M for Pb^{2+}; 3.5×10^{-8} M for Hg^{2+}	S9
5.	MB	0.36 nmol/L for Hg^{2+}; 0.16 nmol/L for Pb^{2+}	S10
6.	Cys-AgNPs	45.39×10^{-9} M for Hg^{2+}; 49.39×10^{-9} M for Pb^{2+}	S11
7.	AgNPs	8.0×10^{-7} M for Hg^{2+}; 2.0×10^{-7} M for Pb^{2+}	S12
8.	DNA-based sensor	10 pM for Pb^{2+}; 0.1 nM for Hg^{2+}	S13
9.	PBA and HBA	0.98 pM for Pb^{2+}; 19 pM for Hg^{2+}	S14
10	poly(2-VP-MBAm-AA)	10 μg L^{-1} for Hg^{2+} & Pb^{2+}	S15
11.	Present Work	8.29 nM for Hg^{2+}; 7.65 nM for Pb^{2+}	-

Table S6. Determination of Hg^{2+} in real water samples with H_2L

Sample	pH	Added Hg^{2+} (μM)	Found Hg^{2+} (μM)	Recovery (%)	RSD (%)
Tap water	6.94	0.1	0.097	97.0	1.40
		0.5	0.496	99.2	
		1.0	0.996	99.6	
River water	7.08	0.1	0.096	96.0	2.08
		0.5	0.497	99.4	
		1.0	0.998	99.8	
Bore well water	7.43	0.1	0.099	99.0	0.31
		0.5	0.493	98.6	
		1.0	0.992	99.2	
Industrial Sewage	7.99	0.1	0.097	97.0	1.47
		0.5	0.496	99.2	
		1.0	0.998	99.8	

RSD = Relative standard deviation

Table S7. Determination of Pb^{2+} in real water samples with H_2L

Sample	pH	Added Pb^{2+} (μM)	Found Pb^{2+} (μM)	Recovery (%)	RSD (%)
Tap water	6.94	0.1	0.099	99.0	0.38
		0.5	0.498	99.6	
		1.0	0.997	99.7	
River water	7.08	0.1	0.098	98.0	0.79
		0.5	0.496	99.2	
		1.0	0.995	99.5	
Bore well water	7.43	0.1	0.099	99.0	0.35
		0.5	0.497	99.4	
		1.0	0.997	99.7	
Industrial Sewage	7.99	0.1	0.096	96.0	2.11
		0.5	0.498	99.6	
		1.0	0.997	99.7	

RSD = Relative standard deviation

REFERENCES

[S1] H. A. Benesi and J. H. Hildebrand, *Journal of the American Chemical Society*, 1949, **71**, 2703-2707;

[S2] A. Mallick and N. Chattopadhyay, *Photochemistry and Photobiology*, 2005, **81**, 419-424;

[S3] P. Roy, K. Dhara, M. Manassero, J. Ratha and P. Banerjee, *Inorganic Chemistry*, 2007, **46**, 6405-6412.

[S4] H. M. Irving, M. G. Miles and L. D. Pettit, *Analytica Chimica Acta*, 1967, **38**, 475-488.

[S5] L. Alderighi, P. Gans, A. Ienco, D. Peters, A. Sabatini and A. Vacca, *Coordination Chemistry Reviews*, 1999, **184**, 311.

[S6] S. Muthusamy, K. Rajalakshmi, D. Zhu, W. Zhu, S. Wang, K. B. Lee, H. Xu and L. Zhao, *Sensors and Actuators B: Chemical*, 2021, **346**, 130534.

[S7] C. Liu, C. Huang and H. Chang, *Analytical Chemistry*, 2009, **81**, 2383-2387.

[S8] Z. Khoshbin, M. R. Housaindokht, A. Verdian and M. R. Bozorgmehr, *Biosensors and Bioelectronic*, 2018, **116**, 130-147.

[S9] Z. Hu, C. Lin, X. Wang, L. Ding, C. Cui, S. Liu and H. Y. Lu, *Chemical Communications*, 2010, **46**, 3765-3767.

[S10] Z. Lu, W. Xiong, P. Wang, X. Li, K. Zhai, R. Shi and D. Xiang, *International Journal of Environmental Analytical Chemistry*, 2021, **101**, 1-13.

[S11] V. R. Samuel and K. J. Rao, *Chemical Physics Impact*, 2023, **6**, 100161.

[S12] F. Ahmed, H. Kabir and H. Xiong, *Frontiers in Chemistry*, 2020, **8**, 1-15.

[S13] Z. Lin, X. Li and H. Kraatz, *Analytical Chemistry*, 2011, **83**, 6896-6901.

[S14] F. Gao, F. Zhan, S. Li, P. A. Mensah, L. Niu and Q. Wang, *Biosensors and Bioelectronics*, 2022, **209**, 114280.

[S15] S7. R. Sedghi, S. Kazemi and B. Heidari, *Sensors and Actuators B: Chemical*, 2017, **245**, 860-867.